Author version: Deep-Sea Research I, vol.57(6); 2010; 739-754

Observed intra-seasonal to interannual variability of the upper ocean thermal structure in the southeastern Arabian Sea during 2002–2008

V. V. Gopalakrishna[1], F. Durand[2,1], K. Nisha[1], M. Lengaigne[6,1],T. P. Boyer[7],J. Costa[1], R. R. Rao[3], M. Ravichandran[4], S. Amrithash[5], L. John[5], K. Girish[5], C. Ravichandran[5] and V. Suneel[1]

[1]National Institute of Oceanography, Dona Paula, Goa, India.

[2]IRD, LEGOS, UMR5566 CNRS-CNES-IRD-UPS, Toulouse, France.

[3]Japan Marine Earth Science & Technology, Yokosuka, Japan.

[4]Indian National Centre for Oceanography Information Services, Hyderabad, India.

[5]National Institute of Oceanography, Regional Centre, Kochi-403004, India.

[6]Laboratoire d'Océanographie et de Climatologie : Expérimentations et Analyses, CNRS, Paris, France.

[7]NOAA National Oceanographic Data Center, Silver Spring, Maryland, USA.

Abstract

The southeastern Arabian Sea (SEAS), located in the Indian Ocean warm pool, is a key-region of the regional climate system. It is suspected to play an important role in the dynamics of the Asian summer monsoon system. The present study reports the salient features derived from a newly harvested observational dataset consisting of repeated fortnightly XBT transects in the SEAS over the period 2002–2008. The fortnightly resolution of such a multi-year record duration is unprecedented in this part of the world ocean and provides a unique opportunity to examine the observed variability of the near-surface thermal structure over a wide spectrum, from intra-seasonal to interannual time scales. We find that most of the variability is trapped in the thermocline, taking the form of upwelling and downwelling motions of the thermal stratification. The seasonal variations are consistent with past studies and confirm the role of the monsoonal wind forcing through linear baroclinic waves (coastally-trapped Kelvin and planetary Rossby waves). Subseasonal variability takes the form of anomalous events lasting a few weeks to a few months and occurs at two preferred time-scales: in the 30–110 day band, within the frequency domain of the Madden-Julian Oscillation and in the 120–180 day band. While this subseasonal variability appears fairly barotropic in the offshore region, the sign of the anomaly in the upper thermocline is opposite to that in its lower part on many occasions along the coast. Our dataset also reveals relatively large interannual temperature variations of about 1°C from 50 m to 200 m depth that reflect a considerable year-to-year variability of the magnitude of both upwelling and downwelling events. This study clearly demonstrates the necessity for sustained long-term temperature measurements in the SEAS.

Keywords: XBT data, Arabian Sea, Lakshadweep Sea, Inter-annual variability, Intra-seasonal variability, WICC.

1. Introduction

The Lakshadweep Sea (henceforth LS), in the southeastern Arabian Sea (SEAS), is of prime climatic importance, being situated in the Indian Ocean warm pool (Fig. 1). It is also an area of marked oceanic dynamical activity. Several hydrographic cruises carried out during different seasons revealed striking contrasts between summer monsoon and winter monsoon seasons (Shetye et al., 1990, 1991). The advent of altimetry in the early 1990s allowed documentation of a clear seasonal cycle in the SEAS, with positive sea level anomaly (SLA) during winter and negative SLA during summer (Shankar and Shetye, 1997; Bruce et al., 1998). This feature was termed the Lakshadweep High and Low (henceforth LH/LL), after the name of the island chain (see Fig. 1 for the typical location and dimension of LH/LL). The LS has a peculiar geographic location: it is situated at low latitude, within the northern Indian Ocean basin (a completely tropical basin, closed at 25°N) and in the vicinity of the eastern boundary of the Arabian Sea. This makes likely a rapid adjustment to the highly variable monsoonal winds. Indeed, the adjustment via tropical baroclinic waves (equatorial Rossby and Kelvin waves, coastal Kelvin waves propagating along the periphery of the northern Indian Ocean, and planetary Rossby waves propagating westward in the interior Bay of Bengal and Arabian Sea) takes place over timescales of a few weeks to a few months for the lowest-order baroclinic modes (McCreary et al., 1993). Over the last 15 years, a hierarchy of numerical studies (McCreary et al., 1993; Shankar and Shetye 1997; Shankar et al., 2002) led to the conclusion that the seasonal variability of LS hydrographic structure can be seen essentially as the linear response of the ocean to seasonally varying winds. The main forcing is exerted by the seasonal cycle of alongshore winds at the western boundary of the Bay of Bengal, it being connected to LS through the coastal Kelvin waveguide. The variability of local alongshore winds (blowing along the coast of south-west India) also has a sensible role on the LS thermohaline variability, though secondary as compared to Bay of Bengal winds (Shankar et al., 2002). This highlights the fundamentally different dynamics at the eastern vs western boundaries of Arabian Sea: the LH/LL regime is not a response to turbulent instability in the ocean, unlike the Socotra eddy seen off Somalia in summer (Schott and McCreary, 2001).

Observations of sub-seasonal variability in our area of interest are extremely scarce. Still, they provide evidence that the seasonally-contrasted sequence of events seen in the previous paragraph is somehow blurred by higher frequencies. Based on the current-meter time series of Schott et al. (1994), Nethery and Shankar (2007) reported a relative maximum of energy at 110 days in the

spectrum of the current observed at 150 m depth, south of Sri Lanka. Based on a 21-month long record of a current meter situated at 15°N, but slightly further offshore at the shelf break, Vialard et al. (2009) showed that the along-shore current at 50 m was highly variable at 2 - 3 - month periods under the remote influence of the equatorial winds. From the analysis of altimetry and eddy-permitting numerical model, Bruce et al. (1998) reported that the SEAS is populated with energetic mesoscale features that introduce some intraseasonal variability in the smooth, seasonal sequence of events described in the previous section.

The literature is even less abundant about the interannual variability of LS thermal structure. Recently, Shankar et al. (2010) analysed the low-frequency variability of sea level in the entire northern Indian Ocean. From linear numerical simulations, they pointed out some fundamental reasons that prevent any remotely-forced variability to exist in the eastern Arabian Sea at multi-year periodicities.

The LS presents the highest SST of the world ocean during the pre-summer monsoon period, with values exceeding 30°C in climatological conditions during April-May (see the review by Shenoi et al. (2005a)). In two quasi-simultaneous studies, Shenoi et al. (1999) and Rao and Sivakumar (1999) analyzed processes conducive to this SST maximum. Both studies invoked the role of upper ocean salinity stratification in the observed SST pattern: during December, LS surface waters freshen because of advection of Bay of Bengal water by the East India Coastal Current and the Winter Monsoon Current. This low-salinity cap induces a thinning of the mixed layer, thereby diminishing the thermal inertia of the upper ocean as compared to the surrounding ocean. This, together with the downwelling forcing from the coastal waveguide occurring during October-January, limits vertical mixing with the underlying cooler water, and thus inhibits the dissipation of the SST high. Under the effect of radiative heat input, this conjunction of events favours the build-up and maintenance of a distinct SST pattern popularly known as the “Mini Warm Pool” (Rao and Sivakumar 1999). The exact role of ocean processes in the Mini Warm Pool build-up was further investigated using several oceanic models, but results remain controversial (see the review by Vinayachandran et al., 2007). While Durand et al. (2004) concluded that the ocean plays a prominent role in the SST rise during the pre-summer monsoon season, through the trapping of heat in the barrier layer, Kurian and Vinayachandran (2007), on the contrary, concluded that the SST high results essentially from the structure of the atmospheric fluxes, there being a local minimum of latent heat loss in the SEAS during winter.

The SSTs in excess of 30°C in April-May in the SEAS are well above the commonly accepted threshold of 28°C for the triggering of deep atmospheric convection (Graham and Barnett, 1987). This has fostered a number of studies on the possible role of the LS in the ocean-atmosphere interactions and onset of summer monsoon (see the review by Vinayachandran et al., 2007). Rao and Sivakumar (1999) and Shenoi et al. (1999) suggested that the Mini Warm Pool of the LS favours the development of an atmospheric vortex in May-June, the so-called monsoon onset vortex, conducive to monsoon onset over southern India. Considerable controversy still exists among the atmospheric community about the year-to-year repetitiveness of this atmospheric feature, about the exact role of the ocean in its genesis, and about the role of the vortex in the larger context of the dynamics of the summer monsoon. The only ocean-atmosphere coupled modelling study that specifically addressed the role of the LS in the southwestern Asian climate was by Masson et al. (2005). They concluded that salinity stratification in the LS exerts a strong constraint on the SST budget during the pre-summer monsoon season, which in turn controls the timing and intensity of subsequent monsoonal rains over southern India. Their conclusion, however, relies on a coarse resolution ocean-atmosphere model and needs to be checked with an up-to-date system.

In view of the large dynamic variability of this region, under the aegis of the Indian climate research program, the Arabian Sea Monsoon Experiment field program was conceived, planned and executed in the LS to understand the coupling between the summer monsoon and the upper ocean. Under this program, repeat XBT transects were carried out in the LS in a systematic manner during 2002–2008. This constitutes an unprecedented observational effort in this part of the world ocean. A few studies have already been published that used limited subsets of the present dataset. They dealt only with the thermal structure of the surface mixed-layer and its link with sea surface salinity variability (Gopalakrishna et al., 2005; Nisha et al., 2009). Only the study by Gopalakrishna et al. (2008) explicitly dealt with the thermal variability of the upper 150 m of the water column, but focusing on the 2002–2005 period only. In the present paper, our goal is to showcase systematically and exhaustively the basic features of ocean temperature variability in the upper 200 m of LS, considering the May 2002–May 2008 period.

2. Data and processing

Our dataset consists of repeated XBT transects in the LS. Near-fortnightly XBT surveys have been quasi-continuously conducted since May 2002 using passenger ships that ply regularly between Kochi and Lakshadweep Island Chain (Fig. 1). During each XBT survey, a minimum of ten to

thirteen vertical temperature profiles (T7 Sippican XBT probes and MK21 data acquisition system) are collected, at 50- km nominal spatial intervals. The depth of the XBT temperature measurements was calculated using the Hanawa et al. (1995) drop rate equation. Black dots in Fig. 1 locate the XBT stations. Over the May 2002–May 2008 period, 1324 vertical temperature profiles were collected. The Kochi–Kavaratti (KK), on the northern flank of the LH/LL, and Kochi–Minicoy (KM), cutting through the coastal flank of LH/LL, are the most densely covered transects (shaded strips in Fig. 1), with 783 and 249 XBT profiles, respectively. The Kavaratti–Minicoy (north-south) transect is less intensely sampled because of limited availability of passenger ships and is not utilised in the present study. The spatio-temporal distribution of data along KK and KM transects is shown in Fig. 2. It is important to notice the high level of homogeneity of the data coverage on both routes throughout the 6-year-long period of measurements. Typically, for the KK transect all signals of scale of order 1° and 1 month are adequately resolved. In several instances a nominal resolution of 0.5° and 15 days is achieved. Along the KM route, the typical resolution is of order 1° and 1 season.

The XBT data are processed and quality controlled following the procedures laid down in Bailey et al. (1994). XBT profiles pertaining to individual cruises were plotted and subjected to physical verification to examine consistency among the profiles, identifying genuine temperature inversions and sharp spikes. These profiles were also compared with the corresponding climatological profile of the region, taken from World Ocean Atlas (WOA2005; Locarnini et al., 2006), as well as with the climatology developed using the present six-year XBT dataset. Further, in order to compensate for the response time of the thermistor (temperature sensor in the XBT probe) the SST value is replaced by the temperature at 4.5 m depth. All the suspected XBT profiles were discarded. These amounted to 9% of the total number of profiles. This is comparable to the performance typically achieved in other parts of the world ocean. The irregularly distributed dataset was re-gridded on a regular 0.5° longitude × 1 month grid. XBT profiles falling in each 0.5° longitude box were grouped together to generate an average profile and placed at the middle of each box. Irrespective of the XBT cruise period (which sometimes reached two months), monthly means were generated considering the profiles corresponding to a given month. This gridding procedure in space and time was followed to generate all the parameters used in the present analysis for both KK and KM transects.

3. Mean upper ocean thermal structure

Fig. 3a presents the mean temperature of the upper 200 m along the KK route. It is very similar along the KM route (not shown). Very warm waters (temperature above 28°C) are found in the upper 40 m. Peak SST exceeds 29°C west of 73.5°E. Above the core of the thermocline, isotherms upslope gently towards the coast, from about 73°E. This is consistent with the known southward (and thus upwelling-favourable) direction of the alongshore component of the wind throughout the seasonal cycle over the southwest coast of India (Schott and McCreary, 2001). Variability around this mean structure strikingly appears trapped in the thermocline, with values of standard deviation typically in excess of 3°C (Fig. 3b). It is much weaker in the mixed layer and in the subthermocline, with values near or lower than 1°C. Fig. 3c presents the longitudinal section of the maximum standard deviation seen in Fig. 3b. The standard deviation is maximum at 75°E, viz. in the shelf break area, where it almost reaches 4°C. It decreases westward down to 3°C at the western edge of the transect. Visual comparison of Figs. 3a and 3b shows that the maximum variability is roughly seen at the depth of the thermocline. The thermocline trapping of thermal variability suggests the dominance of dynamically-driven temperature variability over thermodynamic processes. Assuming that all the observed variability can be represented in terms of vertical movements of the thermal stratification, it is interesting to compute the equivalent amplitude of the vertical movement corresponding to the observed thermal variability. In this idealized case, the standard deviation Dz of the depth of a given isotherm is simply given by :

$$Dz = \frac{DT}{\P T \P z} \quad (1)$$

where DT is the standard deviation of temperature shown on Fig. 3b, and $\P T \P z$ is the background vertical gradient of temperature at this particular location. At every longitude and at the depth of maximum variability seen on Fig. 3b, we computed this equivalent vertical displacement (Fig. 3d). As in Fig. 3c, we note a westward drop of the equivalent displacement. It is maximum at the eastern edge of the transect, at the shelf break, with values exceeding 60 m. It decreases continuously to 72.75°E, where it amounts to only 20 m. The very sharp decrease in the offshore direction is due to the combined effect of a drop of the maximum temperature variability seen on Fig. 3c (the numerator of (1)) and a rise of the vertical gradient of temperature seen on Fig. 3a (the denominator of (1)). Interestingly, the longitudinal profile of Dz is very suggestive of an exponential with e-folding scale of about 1.5°. In the framework of linear dynamics, the theoretical

value of Dz is one Rossby radius of deformation (Gill, 1982). It amounts to approximately 100 km in the LS for the first baroclinic mode, as seen in Chelton et al. (1998). The broad consistency between our empirical estimate and the theoretical value echoes the known validity of linear physics in explaining the basic dynamical features of the LS (Shankar et al., 2002).

4. Annual cycle of the thermal structure

4.1 Comparison with existing climatology

Fig. 4 presents the monthly climatology of thermal structure along the KK route extracted from WOA2005 as well as from our new dataset. For clarity we also plotted their difference (obtained by substracting our dataset from WOA2005). Clearly, our dataset is broadly consistent with WOA2005, with a salient seasonal signal composed of upwelling from May to August, downwelling from October to February, and minimum variations during the intervening periods. The typical temperatures in the mixed layer, in the thermocline and deeper are also similar in the two datasets throughout the seasonal cycle. A closer examination, however, reveals interesting differences between the two datasets. First, our XBT dataset exhibits a steeper east-west slope of the isotherms during both upwelling and downwelling seasons. This is revealed by the sign of their difference: during the upwelling season (May-August), it is systematically positive at thermocline depth in the eastern half of the transect, with predominantly negative values in the western half from June to August; during the downwelling season, the situation is reversed, our dataset being consistently warmer than WOA2005 at thermocline depth in the east. We can not rule out the different time span of the two climatologies (the whole 20th century for WOA2005 vs. 2002–2008 for our dataset) in explaining some aspects of their difference. In particular, this could be the reason why WOA2005 is quasi-systematically cooler than our dataset in the mixed layer. However, the pattern of their difference, with its seasonal dependency, strongly points to the different resolution between the two fields: while our XBT dataset has an actual resolution of 0.5° (Fig. 2 and Section 2), WOA2005 has a nominal resolution of 1° only, and probably even less because of the longer correlation scales used in their gridding procedure.

4.2 Seasonal evolution of the thermal field

In the following, we consider the 25°C isotherm depth (henceforth noted D25) as a proxy for thermocline depth. At the end of the upwelling season in August, the thermocline lies at 10 m at 75.75°E and at 70 m at 72.25°E. This denotes the West India Coastal Current flowing equatorward at

the surface (Schott and McCreary, 2001). Then the downwelling season starts: the thermocline deepens in September until November, when it reaches its deepest position at 110 m at 75.75°E. During this period, the West India Coastal Current slows down (in August-September) and turns to flow poleward from October onward. Subsequently, thermocline depth increases, but only in the western part of the transect. This is consistent with the known westward propagation of the coastal trough as a Rossby wave at this time of the year (Shankar and Shetye, 1997). By February the thermocline is roughly flat (at about 100 m) all along the transect, and the West India Coastal Current reverses again. In April the upwelling has started, with thermocline shoaling to 75 m at 75.75°E. This corresponds to an equatorward West India Coastal Current. The thermocline continues shoaling through July in the east. In the west, the thermocline uplifting is delayed and starts in June only. This is also consistent with the westward propagation of the coastal crest expected there (Shankar and Shetye, 1997). From July to September, during the upwelling season, our dataset reveals a downwelling below the thermocline, as seen from the downward slanting of the 18°C isotherm towards the coast, at the eastern edge of our section (east of 74.5°E). This corresponds to a poleward undercurrent, underlying the equatorward West India Coastal Current. Such a sheared structure, typical of eastern boundary regimes, was observed by Shetye et al. (1990) from hydrographic surveys of the SEAS, with similar vertical and zonal position.

Unlike many other eastern boundaries of the world ocean, the seasonal cycle of thermocline depth in the LS described above is puzzling because it leads the local wind forcing by several months. This is explained by the fact that the LS is at an eastern oceanic boundary but directly connected to the western boundary of the Bay of Bengal (via the coastal Kelvin waveguide of the Indian subcontinent). The exact mechanisms forcing the seasonal variability of the thermocline depth (and, thus, of the West India Coastal Current) in the LS was ascertained by the numerical studies of McCreary et al. (1993) and Shankar et al. (2002). It turns out that the downwelling phase (conducive to the LH in winter) is chiefly driven by the seasonal cycle of the alongshore winds in the western and northern Bay of Bengal (primarily by the collapse of the monsoonal winds there, in late summer-early fall). The upwelling phase (resulting in the LL in summer) is locally forced by the southward alongshore wind during winter monsoon, even though the western Bay of Bengal winds also remotely contribute to it.

4.3 Variability of SST, thermocline depth and mixed-layer depth

4.3.1. SST

The SST in the LS presents a semi-annual behaviour, with high values (in excess of 29°C) during spring and fall intermonsoons and lower values during summer and winter monsoons (Fig. 5a). The evolution along the KM route is very similar to that along the KK route, though with slightly weaker extrema in the central part of the domain (Fig. 5b). de Boyer Montégut et al. (2007a) carried out a SST budget of the whole eastern Arabian Sea from a numerical model output. They concluded that the atmospheric forcing dominates the SST evolution throughout the seasonal cycle in agreement with Rao and Sivakumar (2000). This is also what our observations suggest for the particular case of the SEAS embedded in their larger domain. It is indeed interesting to note the decoupling between SST and subsurface temperature evolution on Fig. 4. For example, SST rises sharply during the pre-summer monsoon season, under the combined effect of strong solar radiation and reduced latent heat loss (Sengupta et al., 2002); during the same period, the underlying thermocline waters strongly cool under the dynamic effect of upwelling. de Boyer Montégut et al. (2007a) suggest that a small part of this subsurface cooling does affect the SST evolution, but it remains largely dominated by the atmospheric heating (see their Figure 3b). Only the secondary SST rise in October-November mirrors the subsurface warming during this period. This, though, corresponds to two different mechanisms (de Boyer Montégut et al., 2007a): the surface heats up because of increased atmospheric heat flux, whereas the thermocline waters are dynamically downwelled (see Section 3). The SST cools quickly with the onset and progress of the summer monsoon, under the effect of latent heat loss (de Boyer Montégut et al., 2007a).

4.3.2. Thermocline depth

The signature of baroclinic waves (upwelling/downwelling Rossby wave in summer/winter) in setting up the observed variability is seen in the observed westward propagation of the patterns seen at the eastern edge of the routes sampled. Along the KK route, for example, the summer uplifting of D25 is maximum in August at 75.25°E and is delayed to October at 72.75°E (Fig. 5a). This corresponds to a phase velocity of about 5 cm/s, roughly consistent with the theoretical speed of a mode-2 or mode-3 Rossby wave at this latitude. A similar value is observed in the numerical simulation of Shankar and Shetye (1997). A modal decomposition carried out in the ocean general circulation model of Durand et al. (2004) confirmed that, in their simulation of the seasonal

variability of the SEAS thermal structure, the combined contributions of 2nd and 3rd baroclinic modes dominate over that of 1st baroclinic mode. Given the shallow MLDs existing in the area, as well as in the Bay of Bengal, the wind forcing appears as a good candidate to explain this dominance of higher-order baroclinic modes over the 1st one in our area. Along the KM route the same kind of propagation is also visible, though with an increased apparent phase speed (Fig. 5b): the minimum D25 is also seen in August at 75.25°E, but as early as September at 73.25°E. This faster propagation speed is consistent with a higher Rossby wave speed at 9°N (the mean latitude of KM route) as compared to 10.5°N (the mean latitude of KK route), though the monthly sampling of our interpolated dataset does not allow an accurate estimation of the propagation speed. Along the KK route, the peak-to-peak excursion of D25 reaches 90 m at the eastern edge of the transect. This value decreases westward to about 40 m at 72.5°E. This is in line with the westward decrease of equivalent displacement discussed in Section 3 (Fig. 3d).

4.3.3. Mixed layer depth

The mixed layer depth (henceforth MLD) is defined as the depth where the temperature is 0.5°C lower than SST. One must keep in mind that this depth might overestimate the actual MLD, as salinity stratification is notorious for limiting the density-mixed layer depth in the SEAS, particularly during the winter season (Rao and Sivakumar, 2003, Durand et al., 2004; Shankar et al., 2004; Shenoi et al., 2004; Gopalakrishna et al., 2005; Durand et al., 2007; de Boyer Montégut et al., 2007b; Mignot et al., 2007). However, the absence of subsurface salinity observations in our area precludes the definition of a density-based criterion. We thus define MLD from temperature only. Along the KK route, MLD shows a contrasted evolution from east to west, with an apparent annual periodicity dominant in the east (close to the shelf) and a semi-annual periodicity in the west (Fig. 5a). In the east the MLD is at its deepest in January (more than 90 m). Then it shoals continuously to reach less than 20 m in August. Afterwards it deepens again until January. In the west, similarly, it is also at its deepest (more than 60 m) in January. The spring shoaling, however, stops in April-May there, when it touches 40 m. During the monsoon it deepens again to reach 60 m in August. Subsequently it shoals during fall to about 40 m in November. MLD evolution along the KM route also shows the same east/west contrast (Fig. 5b), with similar patterns and magnitude of the seasonal cycle. This east/west contrast suggests different mechanisms east and west of 74.5°E. In the east, within the coastal waveguide, MLD variability seems to be driven primarily by vertical movements of the thermocline. It is interesting to note the westward propagation of MLD shoaling in August-

October along the KK route, similar to the propagation of thermocline downwelling during the same period. We can also see a hint of this westward propagation of MLD after monsoon along the KM route, though less clearly. On the contrary, further offshore the diabatic effects seem to play a prominent role during summer; these may consist of buoyancy forcing by the atmospheric fluxes (latent heat loss under the effect of monsoonal winds, see McCreary and Kundu (1989) and de Boyer Montégut et al. (2007a)) or wind-driven entrainment (Fischer et al., 2002).

5. Interannual and intra-seasonal variability

5.1 Non-seasonal variability

In the following, we term as non-seasonal variability the residual signal obtained after removing the seasonal climatology from the raw data. As shown on Figure 6, the non-seasonal variability of temperature is confined at thermocline depth (Fig. 6). The standard deviation shows values in excess of 1.5°C in the central part of the transect, located between 40 m and 120 m. Visual comparison of Fig. 3b and 6 tells that in this depth range, the non-seasonal variance amounts to about one third of the overall variance.

In order to investigate whether there is any seasonality of this non-seasonal variability, the monthly standard deviation of the non-seasonal anomaly of temperature has also been computed along the along the KK route (Fig. 7). This figure thus features the seasonal evolution of the standard deviation plotted on Figure 6. It shows that, irrespective of the season, the variability is consistently trapped in the thermocline. Indeed, it is strongest (typically in excess of 1.5 °C) around 100 m in winter, at the height of the downwelling season; conversely, it is strongest around 50 m in the summer monsoon, once the seasonal upwelling has developped. This figure also suggests that the non-seasonal variability is strongest in summer-fall. Only during this period do standard deviations in excess of 2.5°C appear, mainly in the central and western part of the transect.

Further details of the non-seasonal variability can be inferred from Fig. 8, which displays the temperature evolution for the two selected red boxes shown on Figure 1 (E and W boxes). Clearly, the seasonal periodicity dominates the variability. The peak-to-peak displacement of D25 and D20 between winter and summer season, every year, typically amounts to 80 m / 50 m for E box / W box. This is also consistent with the equivalent displacement plotted on Fig. 3d. Superimposed on this annual cycle, energetic anomalous events stand out at both locations, as reflected by the short-lived vertical excursions of the thermal strucutre, with typical duration of a few weeks.

To separate out the sub-seasonal from the interannual variability, we applied a 200-day running mean to the time series at each depth. This low-frequency evolution of temperature will be referred to as the interannual variability in the following, while the difference between the non-seasonal variability and this low-frequency evolution will be referred to as the sub-seasonal variability.

5.2 Sub-seasonal variability

Fig. 9 presents the time series of sub-seasonal temperature anomalies for the two selected locations (E and W boxes, see Fig. 1). In line with Figs. 6 and 7, the anomalies are quasi-systematically trapped between the bottom of the mixed layer and the bottom of the thermocline (as defined by D20) in W box. The vertical profile of the anomalous patterns is not always homogenous. They appear fairly barotropic for W box throughout the 2002–2008 period. On the contrary, in E box, the sign of the anomaly in the upper thermocline is opposite to that in its lower part on many occasions. This suggests that the linear processes driven by low-order baroclinic modes (which are roughly barotropic within this depth range) may not be the sole contributor to the observed variability. The role of the other mechanisms (instabilities, higher-order baroclinic modes, diabatic processes) is not clear and needs to be ascertained with a dedicated numerical approach. Our data thus suggest different mechanisms of thermal variability, between the shelf break area (where E box is located) and the deep ocean (where W box is). Hydrographic cruises carried out in the area also evidenced a depth-dependent structure in the vicinity of the shelf break (Shetye et al., 1990).

We temporally interpolated D20 and D25 timeseries on a regular bimonthly time axis and computed their power spectrum (Fig. 10). It shows that the sub-seasonal variability occurs at two preferred time scales. In the 30-110-day band, significant peaks are evident in the eastern box. These peaks are within the time frequency domain of the Madden-Julian Oscillation (MJO; Zhang 2005), a large-scale perturbation of atmospheric deep convection with energetic fluctuations of surface winds at periods of 30-90 days. Vialard et al. (2009) indeed revealed that the currents and sea-level variations observed at these time scales along the coast of Goa (about 400 km to the north of our area) are part of basin-scale fluctuations of the northern Indian ocean equatorial and coastal wave guide in response to intraseasonal winds associated with the MJO. These spectra also reveal a second distinct and energetic peak between 110-200-day periods. This peak lies at the low-frequency end of the sub-seasonal variability, and further investigations are required to understand the processes driving this variability.

5.3. Interannual variability

Very little is known about the year-to-year variability of subsurface thermal structure in the study region. In a pioneering study based on the first batch of ARGO floats deployed in the central Arabian Sea, Vinayachandran (2004) pointed out that the general belief that the magnitude of summer cooling in the Arabian Sea is linked to the strength of the summer monsoon is an over-simplified view of the real ocean. The duration of the monsoon season can also play a prominent role. de Boyer Montégut et al. (2007a) investigated the mixed layer temperature variability over 1993–2000 using an ocean model. They evidenced the central role of the latent heat flux anomalies in driving the interannual variability of SST in the eastern Arabian Sea.

Figure 11 displays the interannual temperature variations in the eastern and western boxes. Large low-frequency signals are seen at both locations with amplitude of ~1°C at depth. The vertical profiles of the temperature anomalies appear fairly barotropic in both boxes, extending from the top of the mixed layer to 200 m depth. Consistent with the observations from ARGO floats profiling in the central Arabian Sea (reported by Vinayachandran, 2004), warm anomalies during the summer 2003 are observed, especially in the westen box. Conversely, large negative anomalies are observed during 2007 and to a lesser extent during winter and spring of 2006. A systematic assessment of the mechanism proposed by Vinayachandran (2004) over the whole duration of our observational record is beyond the scope of the present study but forms an interesting perspective.

Fig. 12 displays the longitude-time evolution of D25 for the monthly field along the KK route. It allows further documentation of the interannual variability of the thermocline. It appears that the seasonal sequence of events displayed on Fig. 5 is consistently repeated year after year. The upwelling starts in March off the Indian coast, lasts until August, and is subsequently replaced by downwelling that lasts until January. These signals propagate westward (carried by planetary waves), the western edge of the section showing basically the same evolution as the eastern edge with a 2-month lag. Notable exceptions occur on several occasions, when the propagation of the coastal signal does not extend far offshore or is interrupted at some longitude before re-appearing further to the west (winter 2003–2004, winter 2005–2006 and summer 2007). Throughout the period, the magnitude of the coastal signal decays during the westward propagation, consistent with the westward decrease of the standard deviation seen in Fig. 3b. Unlike the seasonal timing, there is considerable year-to-year variability of the magnitude of both upwelling and downwelling events. Upwelling appears most intense during summer 2002 (with a thermocline virtually touching the sea

surface in the east, as already seen on Fig. 9a) and least marked during summer 2005 (Gopalakrishna et al, 2008). Downwelling is most intense in winter 2005–2006, with a thermocline deeper than 120 m in January 2006 east of 75°E. This extreme event, however, does not propagate west of 74.5°E, which stands in contrast to the continuous propagation throughout our domain observed during most of the years. The 2008 downwelling is the least pronounced, with D25 hardly touching 100 m.

6. Role of salinity on the sea-level variations

The LS is subject to extremely large changes in the upper-ocean salinity at seasonal (Rao and Sivakumar, 2003, Delcroix et al., 2005), interannual and intra-seasonal (Gopalakrishna et al., 2005; Nisha et al., 2009) timescales. Based on long-term repeated thermosalinograph measurements encompassing the three tropical oceans, Delcroix et al. (2005) pointed out that the highest variability of sea surface salinity is observed in the LS, with a standard deviation of about 1 in their 20-year-long time series (see their Fig. 23). Basically, the surface waters of the LS freshen in winter, under the influence of Bay of Bengal water advected by the Winter Monsoon Current (Durand et al., 2007) and by East India Coastal Current (Rao et al, 2008); conversely, salinity increases in summer under the influence of Arabian Sea high salinity water advected equatorward by the West India Coastal Current. Extremely fresh anomalies are seen in January–March 2004 and in January–April 2006, with values lower than 33 at the surface throughout the KK transect; on the contrary, salinities in excess of 35.75 appear from April 2006 through August 2006 (Nisha et al., 2009). This salinity drop/rise is conducive to sea level rise/drop, respectively, through the halosteric effect. The seasonal cycle of the halosteric effect along the KK route should interfere constructively with that of the thermosteric effect generated by the vertical motions of the thermocline seen in Section 4. At this stage, it is interesting to assess the relative imprints of temperature and salinity on sea level variability. Fig. 13 presents the evolution of altimetric sea level anomaly (SLA) along the KK route, obtained from AVISO (1996) gridded product (available from http://atoll-motu.aviso.oceanobs.com/). It integrates both temperature and salt effects. We compare it with the evolution of dynamic height anomaly (DHA) along the same route (Fig. 14). The DHA is computed assuming a constant 35 salinity throughout the water column. Thus it accounts for the thermosteric effect only. The DHA is plotted after removal of the 2002–2008 mean DHA corresponding to each grid point. The measurement errors of altimetric SLA are believed to be in the range 2–3 cm in the open ocean (Fu and Cazenave, 2001). As for DHA computed from XBT profiles, the accuracy is better than 2 cm (Wijffels et al., 2008). To the extent of these measurement errors, any difference

between SLA and DHA should thus be attributed to the halosteric effect. Visual comparison of the two figures shows that both SLA (Fig. 13) and DHA (Fig. 14) mirror the D25 evolution seen in Fig. 12: at the coastal edge of the transect, SLA and DHA are negative (less than -12 cm) at the height of the upwelling season (summer), and positive (over + 10 cm) at the height of the downwelling season (winter). This pattern seen at the eastern edge propagates westward, crossing our area in about 2 months, consistent with the Rossby wave speed discussed in Section 4. However, the consistency between SLA and DHA evolution is verified to a certain extent only. On many occasions, upper ocean salinity can be seen as a good candidate to explain their misfit. For example, DHA is less than -21 cm in September 2004, throughout the central part of the section; at this time, SLA hardly reaches -15 cm. This is consistent with the positive halosteric effect expected from the fresh (33.5) sea surface salinity seen there at this time (Nisha et al., 2009). In the same way, SLA exceeds +12 cm in March 2006 all along the transect, when DHA hardly touches +9 cm west of 74°E; this is when sea surface salinity drops below 33, thereby favouring an enhancement of the positive steric effect. On a few occasions, though, sea surface salinity anomalies can not account for the observed differences between DHA and SLA. This is the case, for example, in October 2005, when DHA is less than -15 cm west of 74°E, whereas SLA remains around -10 cm; this is inconsistent with the salty anomaly (36) seen in sea surface salinity there. The reason for this is unclear. In particular, it is hard to distinguish between the measurement error of altimetric sea level and possible subsurface halosteric contribution in the absence of systematic subsurface salinity measurements. Indeed, the LS is known for vigorous haline variability in the thermocline and below (Shankar et al., 2005; Shenoi et al., 2005b).

7. Conclusion

Apart from reviewing the existing knowledge on the issue of upper SEAS thermal variability, the goal of this study is to present and analyze a novel in situ dataset harvested in the LS. It is based on two repeated XBT transects performed systematically at near-fortnightly interval between the Indian mainland and Lakshadweep Islands, under the Arabian Sea Monsoon Experiment field observational program. The resolution along the best-sampled route (KK) is better than 1° × 1 month, systematically during 2002–2008. Along the other route (KM), the resolution is about half as high. Overall, the data coverage is unprecedented in this part of the world ocean.

Our basic conclusion is that the LS temperature presents a broad spectrum of variability, from intraseasonal to interannual timescales. The variability is trapped primarily at thermocline

depth (between 60 m and 100 m), taking the form of vertical movements of the thermal stratification with amplitude of order 60 m. At seasonal timescales, our dataset essentially confirms what was known from the existing literature. In line with the past modeling studies, the variability patterns show the imprint of linear physics (among which the central role played by baroclinic Kelvin and Rossby waves). In addition, the first-of-its-kind resolution of our dataset reveals a rich variety of sub-seasonal anomalous events. They take the form of short-lived signals trapped in the thermocline. This sub-seasonal variability occurs at two preferred time scales: in the 30-110-day band, within the frequency domain of the Madden-Julian Oscillation, and in the 120-180-day band. Interannual temperature anomalies are also observed at depth and reflect a considerable year-to-year variability of the magnitude of both upwelling and downwelling events. The exact forcing mechanisms responsible for the observed subseasonal and interannual variability (locally or remotely wind-driven or generated by oceanic internal turbulence) remain to be ascertained.

SST exhibits relatively minor variability as compared to subsurface temperature. However, even small variations of SST have the potential to exert considerable climatic impact, given that SST continuously hovers around the critical threshold of 28°C, considered as the minimal value needed to sustain deep atmospheric convection. We have seen that the thermocline is upwelled to extremely shallow levels (of order or less than 20 m) on some occasions. Hence, contrary to what is known from the (limited) literature on this issue, we can not exclude a significant role of the ocean subsurface in driving the SST variability. Though it is beyond the scope of the present paper, the present dataset provides an invaluable source of information to quantitatively assess the upper ocean heat budget in this area over the recent period and at all timescales, from intra-seasonal to interannual.

Acknowledgments.

The repeated XBT measurement program in the Lakshadweep Sea is a major long-term ongoing observational initiative supported by the Ministry of Earth Sciences in India through the Indian National Centre for Ocean Information Services (INCOIS). We thank the Lakshadweep Administrator for permitting XBT measurements onboard their passenger ships. Mr. Shamkant Akerkar helped in the preparation of figures. K. Nisha acknowledges the financial support from the Council of Scientific and Industrial Research, India. We thank Jérôme Vialard for useful discussions. Constructive comments from three anonymous reviewers are gratefully acknowledged. This is NIO contribution xxxx.

References

Bailey, R., Gronell, A., Phillips, H., Tanner, E., Meyers, G., 1994. Quality control cook book for XBT data. Report 221, CSIRO Marine Laboratories.

Bruce, J. G., Kindle, J. C., Kantha, L. H., Kerling, J. L., Bailey, J. F., 1998. Recent observations and modeling in the Arabian Sea Laccadive High region. J. Geophys. Res. 103, 7593–7600.

de Boyer Montégut, C., Vialard, J., Shenoi, S. S. C., Shankar, D., Durand, F., Ethé, C., Madec, G., 2007a. Simulated seasonal and interannual variability of mixed layer heat budget in the northern Indian Ocean. J.Clim. 20, 3249–3268.

de Boyer Montégut, C., Mignot, J., Lazar, A., Cravatte, S., 2007b. Control of salinity on the mixed layer depth in the world ocean: 1. General description. J. Geophys. Res., 112, C06011, doi:10.1029/2006JC003953.

Chelton, D. B., deSzoeke, R. A., Schlax, M. G., Naggar, K. E., Siwertz, N., 1998. Geographical variability of the first baroclinic Rossby radius of deformation. J. Phys. Oceanogr. 28, 433–460.

Delcroix, T., Dessier, A., Gouriou,Y., McPhaden, M., 2005. Time and space scales for sea surface salinity in the tropical oceans. Deep-Sea Res. I. 52, 787–813.

Durand, F., Shetye, S. R., Vialard, J., Shankar, D., Shenoi, S. S. C., Ethe, C., Madec, G., 2004. Impact of temperature inversion on SST evolution in south eastern Arabian Sea during pre-summer monsoon season. Geophys. Res. Lett. **31,** L01305 10.1029/ 2003GL018906.

Durand, F., Shankar, D., de Boyer Montegut, C., Shenoi, S. S. C., Blanke, B., Madec, G., 2007. Modeling the barrier-layer formation in the southeastern Arabian Sea. J.Clim. 20, 2109–2120.

Fu, L.-L. and Cazenave, A., 2001. Satellite Altimetry and Earth Sciences. A Handbook of Techniques and Applications. Academic Press, 463 pp.

Fischer, A. S., Weller, R. A., Rudnick, D. L., Eriksen, C. C., Lee, C. M., Brink, K. H., Fox, C. A., Leben, R. R., 2002. Mesoscale eddies, coastal upwelling, and the upper-ocean heat budget in the Arabian Sea. Deep Sea Res. II, 49, 12, 2231–2264.

Gill, A. E., 1982. Atmosphere-Ocean Dynamics, Volume 30, Academic Press, 662 pp.

Graham, N. E., Barnet, T.P., 1987. Sea surface temperature, surface wind divergence and convection over tropical oceans. Science, 238, 657–659.

Gopalakrishna, V. V., Johnson, Z., Salgaonkar, G., Nisha, K., Rajan, C. K., Rao, R. R., 2005. Observed variability of sea surface salinity and thermal inversions in the Lakshadweep Sea during contrast monsoons. Geophys. Res. Lett. 32, L18605.

Gopalakrishna, V. V., Rao, R. R., Nisha, K., Girishkumar, M. S., Pankajakshan, T., Ravichandran, M., Johnson, Z., Girish, K., Aneeshkumar, N., Srinath, M., Rajesh, S., Rajan, C. K., 2008. Observed anomalous upwelling in the Lakshadweep Sea during summer monsoon season of 2005. J. Geophys. Res. 113, C05001, doi:10.1029/2007JC004240.

Hanawa, K., Rual, P., Bailey, R., Sy, A., Szabados, M., 1995. A new depth-time equation for Sippican or TSK T-7, T-6, and T-4 expendable bathythermographs (XBT), Deep-Sea Res. I, 42, 1423–1451.

Kurian, J., Vinayachandran, P. N., 2007. Mechanisms of formation of the Arabian Sea mini warm pool in a high-resolution Ocean General Circulation Model. J. Geophys. Res. 112, C05009, doi:10.1029/2006JC003631

Locarnini, R. A., Mishonov, A. V., Antonov, J. I., Boyer, T. P., Garcia, H. E., 2006. World Ocean Atlas 2005, Volume 1: Temperature, S. Levitus, Ed. NOAA Atlas NESDIS 61, U.S. Government Printing Office, Washington, D.C., 182.

Masson, S., Luo, J. J., Madec, G., Vialard, J., Durand, F., Gualdi, S., Guilyardi, E., Behra, S., Delecluse, P., Navarra, A., Yamaghata, T., 2005. Impact of barrier layer on winter-spring variability of the southeastern Arabian Sea. Geophys. Res. Lett. 32, L07703.

McCreary, J. P., Kundu, P. K., 1989. A Numerical Investigation of Sea Surface Temperature Variability in the Arabian Sea. J. Geophys. Res. 94, C11, 16,097–16,114.

McCreary, J. P., Kundu, P. K., Molinari, R. L., 1993. A numerical investigation of the dynamics, thermodynamics and mixed layer processes in the Indian Ocean. Progr. Oceanogr. 31, 181–244.

Mignot, J., de Boyer Montégut, C., Lazar, A., Cravatte, S., 2007. Control of salinity on the mixed layer depth in the world ocean: 2. Tropical areas. J. Geophys. Res., 112, C10010, doi:10.1029/2006JC003954.

Nisha, K., Suryachandra Rao, A., Gopalakrishna, V. V., Rao, R. R., Girishkumar, M. S., Pankajakshan, T., Ravichandran, M., Rajesh, S., Girish, K., Johnson, Z., Anuradha, M., Gavaskar, S. S. M., 2009. Reduced near-surface thermal inversions in the Lakshadweep Sea (southeastern Arabian Sea) during winter 2005-2006. J. Phys. Oceanogr., 39, 1184–1199.

Nethery, D., Shankar, D., 2007. Vertical propagation of baroclinic Kelvin waves along the west coast of India. J. Earth Syst. Sci. 116, 331–339, doi:10.1007/s12040-007-0030-6.

Press, W. H., Teukolsky, S. A., Vetterling, W. T., Flannery, B. P., 1992. Numerical Recipes in Fortran 77, The Art of Scientific Computing. Cambridge University Press, 935 pp.

Rao, R. R., Sivakumar, R., 1999. On the possible mechanisms of the evolution of a mini-warm pool during the pre-summer monsoon season and the onset vortex in the southeastern Arabian Sea. Quart. J. Roy. Meteor. Soc. 125, 787–809.

Rao, R. R., Sivakumar, R., 2000. Seasonal variability of the heat budget of the mixed layer and the near-surface layer thermal structure of the tropical Indian Ocean from a new global ocean `temperature climatology. J. Geophys. Res. 105, C1, 995-1015.

Rao, R. R., Sivakumar, R., 2003. Seasonal variability of the salt budget of the mixed layer and near-surface layer salinity structure of the tropical Indian Ocean from a new global ocean salinity climatology, J. Geophys. Res. 108, 3009, doi: 10.1029/2001JC 000907.

Rao, R. R., Girishkumar, M. S., Ravichandran, M., Gopalakrishna, V.V., Thadathil,P., 2008. Observed mini-cold pool south of Indo-Sri Lanka Channel and its intrusion into the southeastern Arabian Sea during winter, Deep-Sea Res.I, 55, 1009– 1020.

Schott, F., Reppin, J., Fischer, J., Quadfasel, D., 1994. Currents and transports of the Monsoon Current south of Sri Lanka. J. Geophys. Res. 99, 25127–25141.

Schott, F., McCreary, J. P., 2001. The monsoon circulation of the Indian Ocean. Progr. Oceanogr. 51, 1–123.

Sengupta, D., Ray, P. K., Bhat, G. S., 2002. Spring Warming of the Eastern Arabian Sea and Bay of Bengal from Buoy Data. Geophys. Res. Lett. 29 (15), 1734, doi:10.1029/2002GL015340.

Shankar, D., Shetye, S. R., 1997. On the dynamics of the Lakshadweep high and low in the southeastern Arabian Sea. J. Geophys.Res. 102, 12,551–12,562.

Shankar, D., Vinayachandran, P. N., Unnikrishnan, A. S., 2002. The monsoon currents in the north Indian Ocean. Progr. Oceanogr. 52, 63–120.

Shankar, D., Gopalakrishna, V. V., Shenoi, S. S. C., Durand, F., Shetye, S. R., Rajan, C. K., Johnson, Z., Araligidad, N., Michael, G. S., 2004. Observational evidence for westward propagation of temperature inversions in the southeastern Arabian Sea. Geophys. Res. Lett. 31, L01305.

Shankar, D., Shenoi, S. S. C., Nayak, R. K., Vinayachandran, P. N., Nampoothiri, G., Almeida,A. M., Michael, G. S., Rameshkumar, M. R., Sundar, D., Sreejith, O. P., 2005. Hydrography of the eastern Arabian Sea during summer monsoon 2002. J. Earth Syst. Sci. 114, 459–474.

Shankar D, Aparna S. G., McCreary, J. P., Suresh, I., Neetu, S, Durand, F, Shenoi, S. S. C, Al Saafani, M. A., 2010. Minima of interannual sea-level variability in the Indian Ocean. Progr. Oceanogr. 84, 3-4, 225-241 .

Shenoi, S. S. C., Shankar, D., Shetye, S. R., 1999. On the sea surface temperature high in the Lakshadweep Sea before the onset of the south-west monsoon. J. Geophys. Res. 104,15,703–15,712.

Shenoi, S. S. C., Shankar, D., Shetye, S. R., 2004. Remote forcing annihilates barrier layer in southeastern Arabian Sea, Geophys. Res. Lett. L05307, doi: 10.1029/2003GL019270.

Shenoi, S.S.C., Shankar, D., Gopalakrishna, V.V., Durand, F., 2005a, Role of ocean on the formation and decay of the core of the warm pool in the southeastern Arabian Sea. Mausam – Indian Journal of Meteorology, Hydrology and Geophysics, 56, 1, 147–160.

Shenoi, S. S. C., Shankar, D., Michael, G. S., Kurian, J., Rameshkumar, M. R., Almeida, A. M., Unnikrishnan, A. S., Fernandes, W., Barreto, N., Gnanaseelan, C., Mathew, R., Praju, K.V., Mahale, V., 2005b. Hydrography and water masses in the southeastern Arabian Sea during March-June 2003. J. Earth Syst. Sci. 114, 475–491.

Shetye, S. R., Gouveia, A. D., Shenoi, S. S. C., Sundar, D., Michael, G. S., Almeida, A. M., Santanam, K., 1990. Hydrography and circulation off the west coast of India during south west monsoon of 1987. J. Mar. Res. 48, 359–378.

Sheyte, S. R., Gouveia, A. D., Shenoi, S. S. C., Michael, G. S., Sunder, D., Almeida, A. M., Sandanam, K., 1991. The coastal currents off western India during northeast monsoon. Deep-Sea Res. A. 38**,** 1517–1529.

Sindhu, B., Suresh, I., Unnikrishnan, A.S., Bhatkar, N.V., Neetu,S., Michael, G.S., 2007. Improved bathymetric datasets for the shallow water regions in the Indian Ocean. J. Earth Syst. Sci. 116, 3, 261-274.

Vialard, J., Shenoi, S. S. C., McCreary, J. P., Shankar, D., Durand, F., Fernando, V. and Shetye, S. R., 2009. Intraseasonal response of Indian-Ocean coastal waveguide to the Madden-Julian Oscillation. Geophys. Res. Lett., 36, L14606, doi:10.1029/2009GL038450.

Vinayachandran, P. N., 2004. Summer cooling of the Arabian Sea during contrasting monsoons. Geophys. Res. Lett. 31, L13306, doi:10.1029/2004GL019961.

Vinayachandran, P. N., Shankar, D., Kurian, J., Durand, F., Shenoi, S. S. C., 2007. Arabian Sea mini warm pool and the monsoon onset vortex. Curr. Sci. 93, 203–214.

Wijffels, S. E., Willis, J., Domingues, C. M., Barker, P., White, N. J., Gronell, A., Ridgway, K., Church, J. A., 2008. Changing expendable bathythermograph fall rates and their impact on estimates of thermosteric sea level rise; J. Clim., 21, 5657–5672.

Zhang, C., 2005. Madden□Julian Oscillation. Rev. Geophys., 43, doi:10.1029/ 2004RG000158.

Figure 1. (top) Mean SST for the Indian Ocean, from WOA2005 climatology. The warm pool (defined as the region of mean SST in excess of 28.5°C) is shaded in red. The black box located in the southeastern Arabian Sea features the limits of our study area. (bottom) Distribution of XBT stations over our study area, during 2002–2008. The 200-m and 1000-m isobaths (taken from Sindhu et al., 2007) are shown. Shaded strips (Kochi-Kavaratti and Kochi-Minicoy) represent the most densely sampled transects. The eastern (E) and western (W) boxes are shaded in red for future reference. Also shown is the typical position of the Lakshadweep High and Low.

Figure 2. Longitude-time distribution of the XBT data along (a) Kochi-Kavaratti and (b) Kochi-Minicoy transects.

Figure 3. Longitude-depth section of (a) the mean and (b) the standard deviation of temperature from the XBT dataset along Kochi-Kavaratti transect. Contours are every 1°C and every 0.5°C for (a) and (b), respectively. (c) Maximal standard deviation as a function of longitude along the Kochi-Kavaratti section. (d) Equivalent vertical displacement (m) at the depth of the maximal standard deviation, as a function of longitude along the Kochi-Kavaratti route (see Section 3 for details).

Figure 4. (a) Longitude-depth sections of monthly climatology of the thermal struture along the Kochi-Kavaratti transect for WOA2005 (left column), for our new XBT dataset (middle column), and their difference (right column) during January to June. (b) Same as (a), during July to December. Isolines are every 5°C for temperature (left and middle columns) and every 1°C for temperature difference (right columns). The months are indicated on each panel of left columns.

Figure 5. (a) Longitude-time sections of monthly climatology of SST (left), mixed-layer depth (middle) and depth of the 25°C isotherm (right), along the Kochi-Kavaratti transect. (b) Same as (a), along the Kochi-Minicoy transect.

Figure 6. Longitude-depth section of standard deviation of temperature anomaly as regards to the monthly climatology, computed over 2002–2008. Contours are every 0.5°C.

Figure 7. Same as Figure 6, computed monthly over the 2002–2008 period. Contours are every 1°C. Superimposed in dashed lines is the monthly climatology of the 25°C isotherm depth.

Figure 8. (a) Time serie of temperature profile observed in E box (contours). Superimposed in thick line is the mixed layer depth. The thin lines feature the depth of the 25°C and 20°C isotherms. The

dots show the XBT data distribution. Gaps longer than 1 month are kept blank. (b) Same as (a), for W box.

Figure 9. (a) Subseasonal variability of temperature profile observed in E box (contours). Superimposed in thick line is the mixed layer depth. The thin lines feature the depth of 25°C and 20°C isotherms. The dots show the XBT data distribution. Gaps longer than 1 month are kept blank. (b) Same as (a), for W box.

Figure 10. Power spectrum of (a) D25 and (b) D20 variation in E box (with seasonal cycle removed) at subseasonal timescales (thick line). (c) and (d) Same as (a) and (b), for W box. The 95% significance level, estimated using autoregressive model fitting, is indicated by dashes.

Figure 11. (a) Interannual variability of temperature profile observed in E box (contours). (b) Same as (a), for W box.

Figure 12. Longitude-time section of 25°C isotherm depth along the Kochi-Kavaratti transect, for the May 2002–April 2008 period. Each panel shows a twelve-month window, from May to the following April. The corresponding year numbers are indicated on each panel. Contours are every 10 m.

Figure 13. Longitude-time section of altimetric sea level anomaly extracted along the Kochi-Kavaratti transect. Contours -10 cm, 0 and 10 cm are drawn in thin line.

Figure 14. Same as figure 13, for the 0-400 m dynamic height anomaly computed from our XBT dataset.

(a) Indian Ocean Climatological Sea Surface Temperature

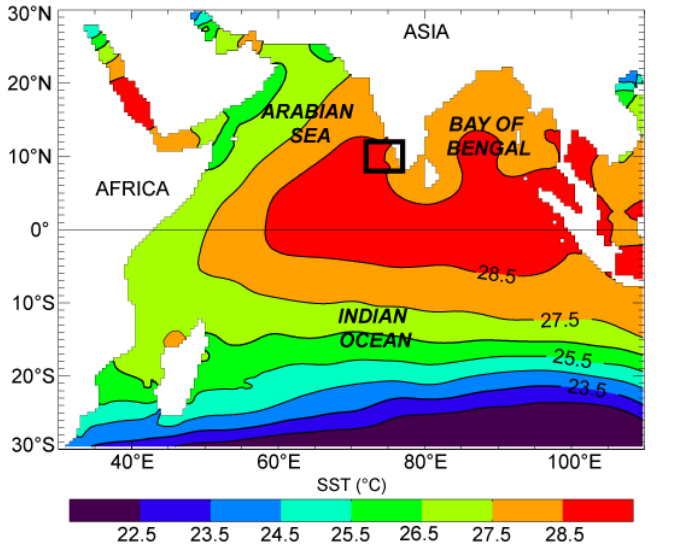

(b) XBT stations in the South-Eastern Arabian Sea

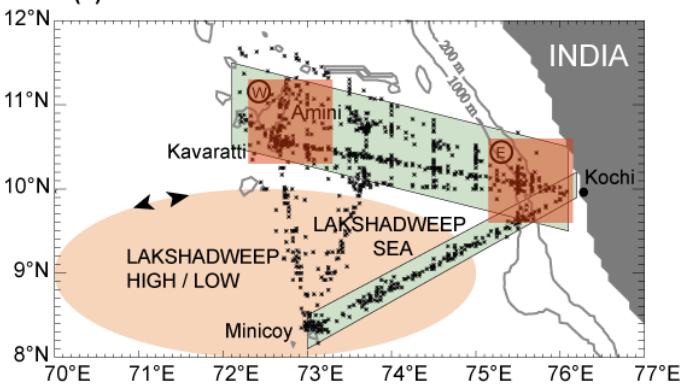

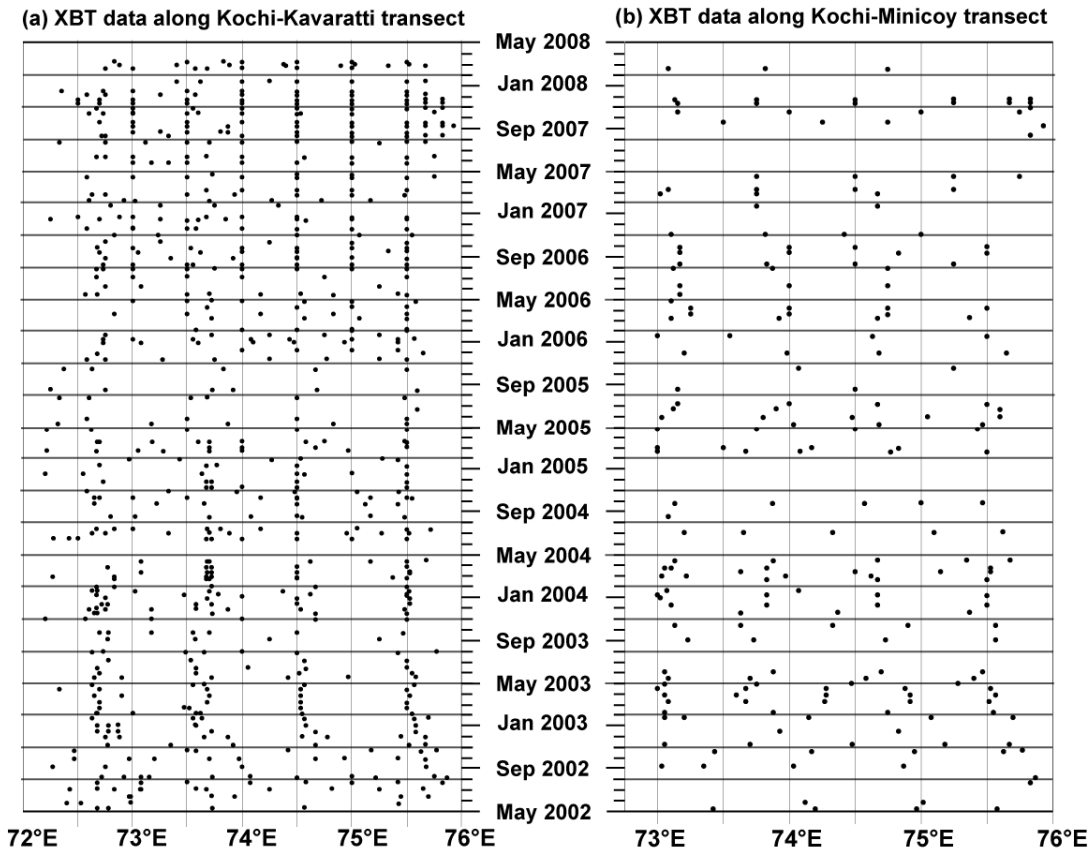
(a) XBT data along Kochi-Kavaratti transect
(b) XBT data along Kochi-Minicoy transect
May 2008
Jan 2008
Sep 2007
May 2007
Jan 2007
Sep 2006
May 2006
Jan 2006
Sep 2005
May 2005
Jan 2005
Sep 2004
May 2004
Jan 2004
Sep 2003
May 2003
Jan 2003
Sep 2002
May 2002
72°E
73°E
74°E
75°E
76°E
73°E
74°E
75°E
76°E

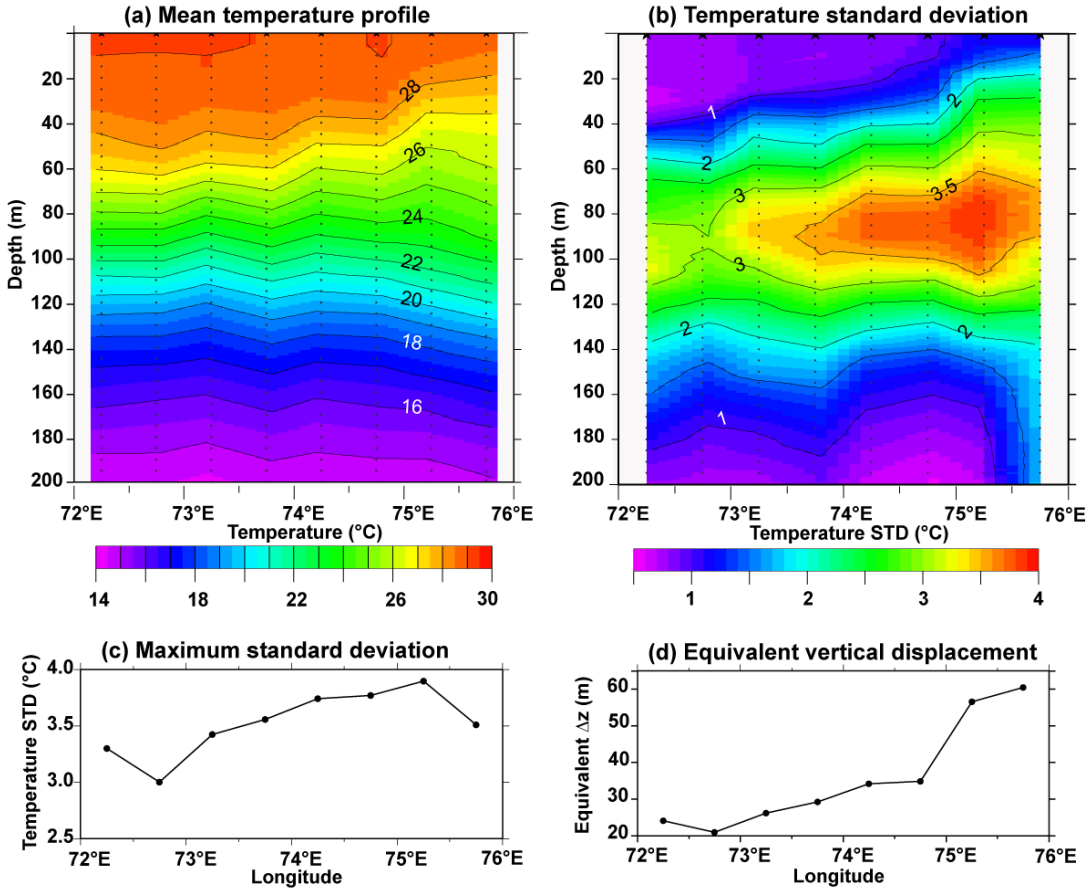
(a) Mean temperature profile
Depth (m)
Temperature (°C)
(b) Temperature standard deviation
Temperature STD (°C)
(c) Maximum standard deviation
Temperature STD (°C)
Longitude
(d) Equivalent vertical displacement
Equivalent Δz (m)
Longitude

Monthly climatology of temperature profile from WOA2005 and the XBT dataset

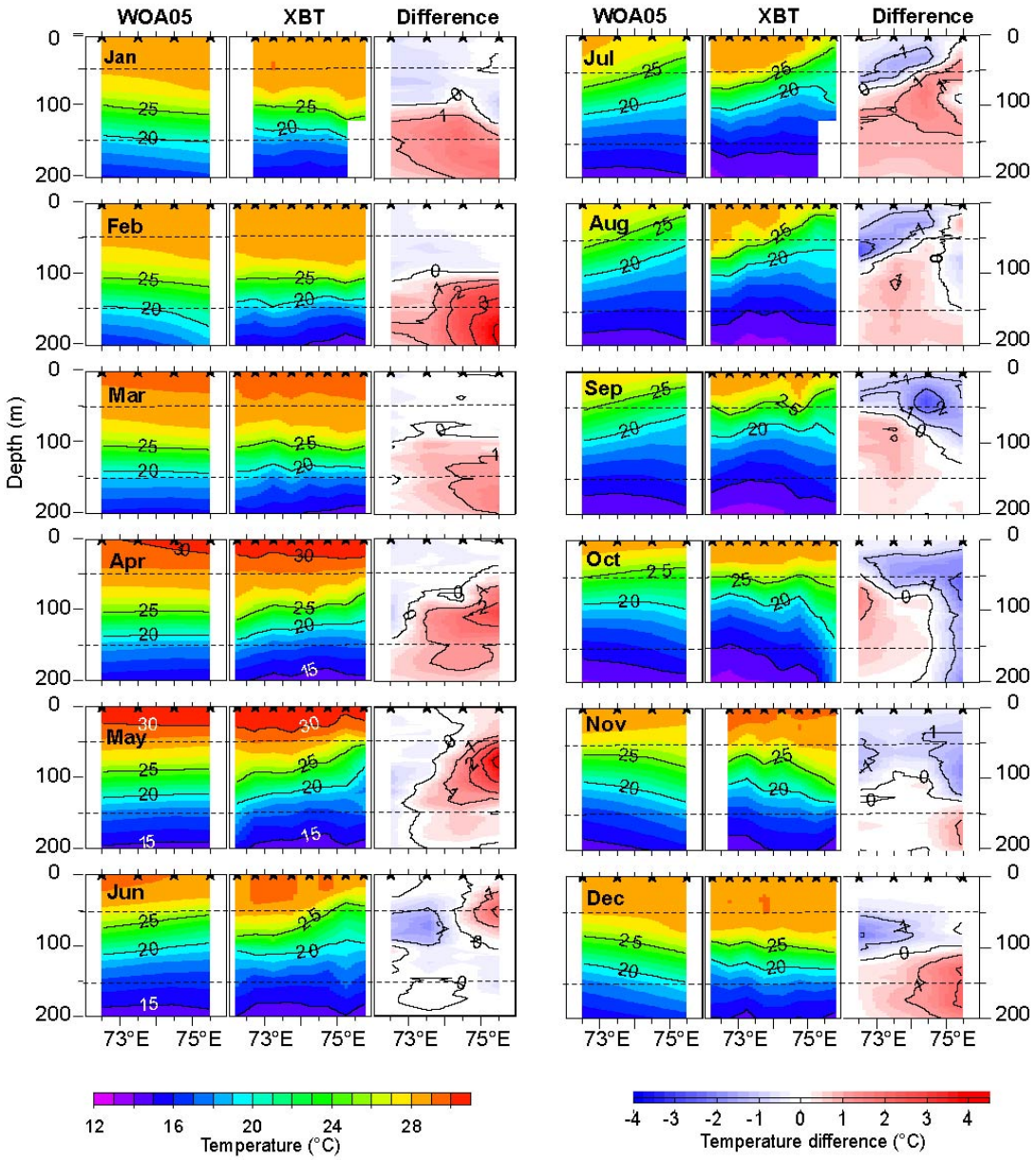

(a) Seasonal cycle of SST, MLD and D25 along Kochi-Karavatti transect

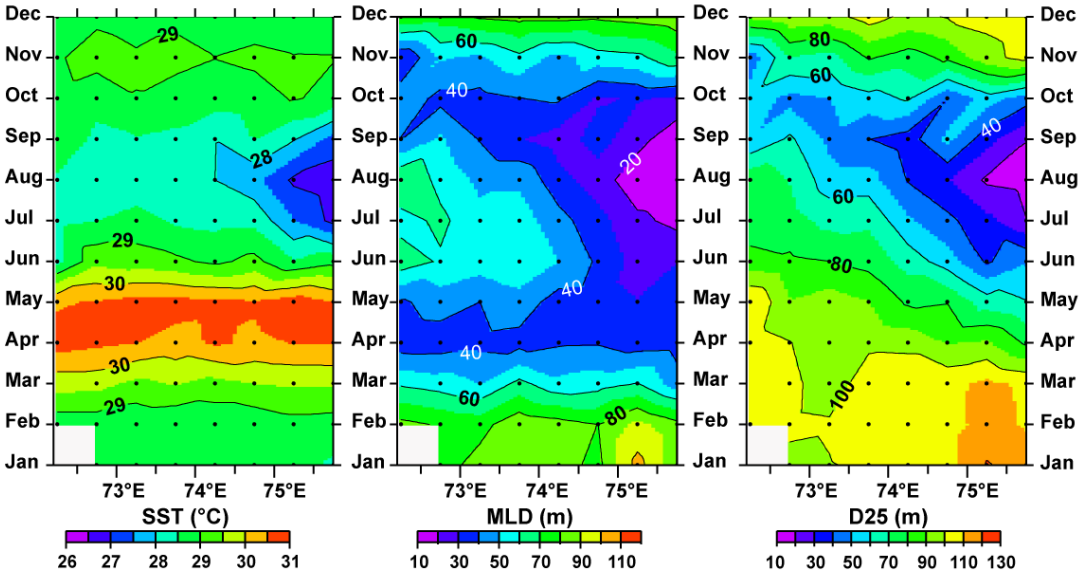

(b) Seasonal cycle of SST, MLD and D25 along Kochi-Minicoy transect

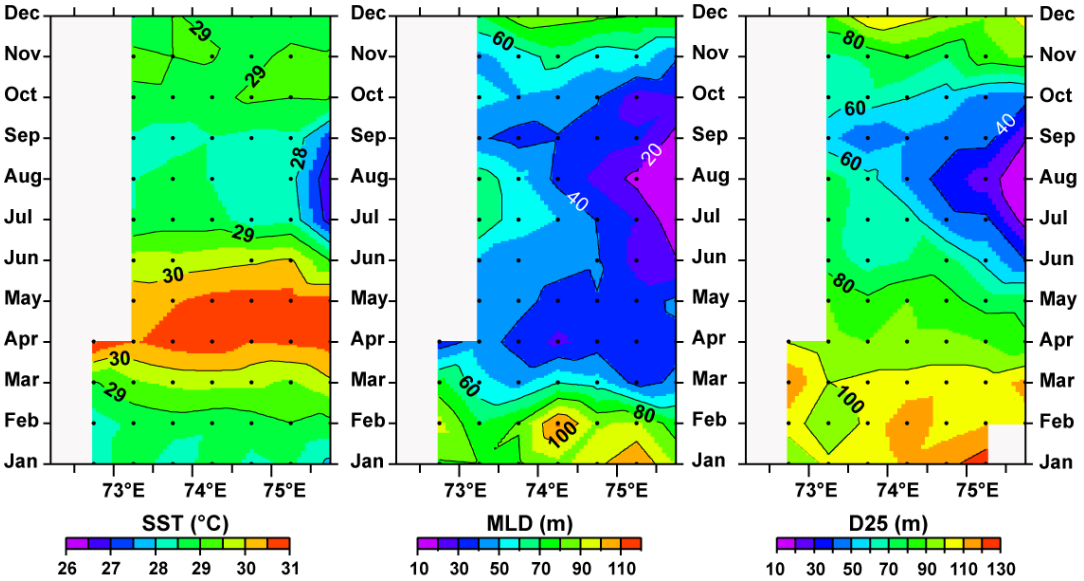

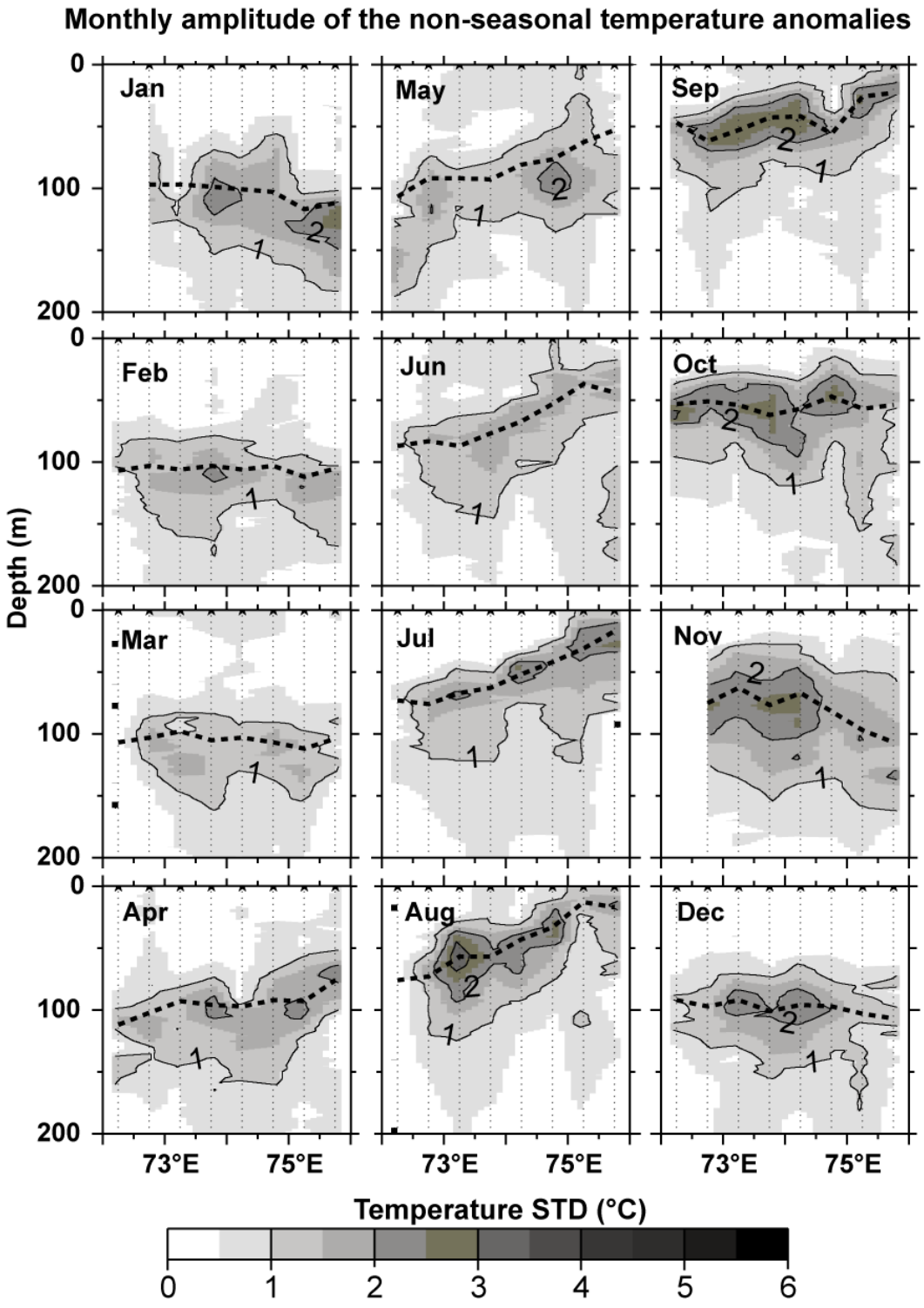
Monthly amplitude of the non-seasonal temperature anomalies
Jan
May
Sep
Feb
Jun
Oct
Mar
Jul
Nov
Apr
Aug
Dec
Depth (m)
0
100
200
73°E
75°E
Temperature STD (°C)
0
1
2
3
4
5
6

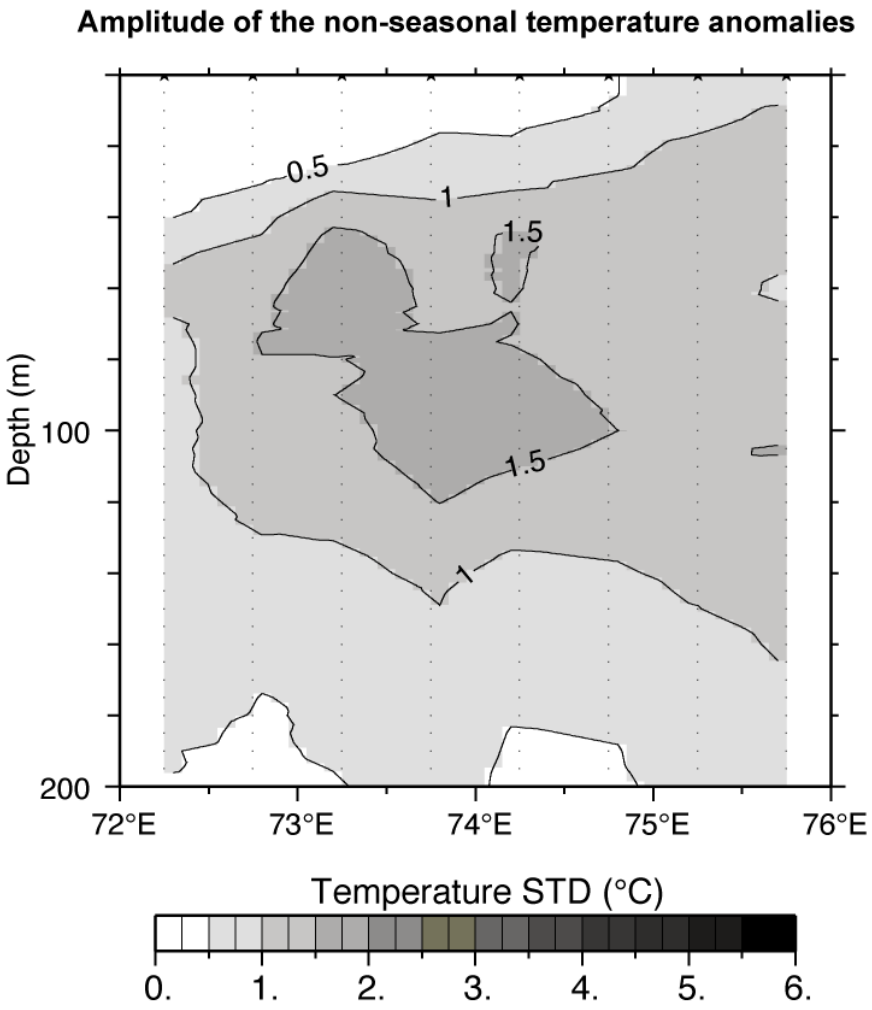
Amplitude of the non-seasonal temperature anomalies
0.5
1
1.5
1.5
1
Depth (m)
100
200
72°E
73°E
74°E
75°E
76°E
Temperature STD (°C)
0.
1.
2.
3.
4.
5.
6.

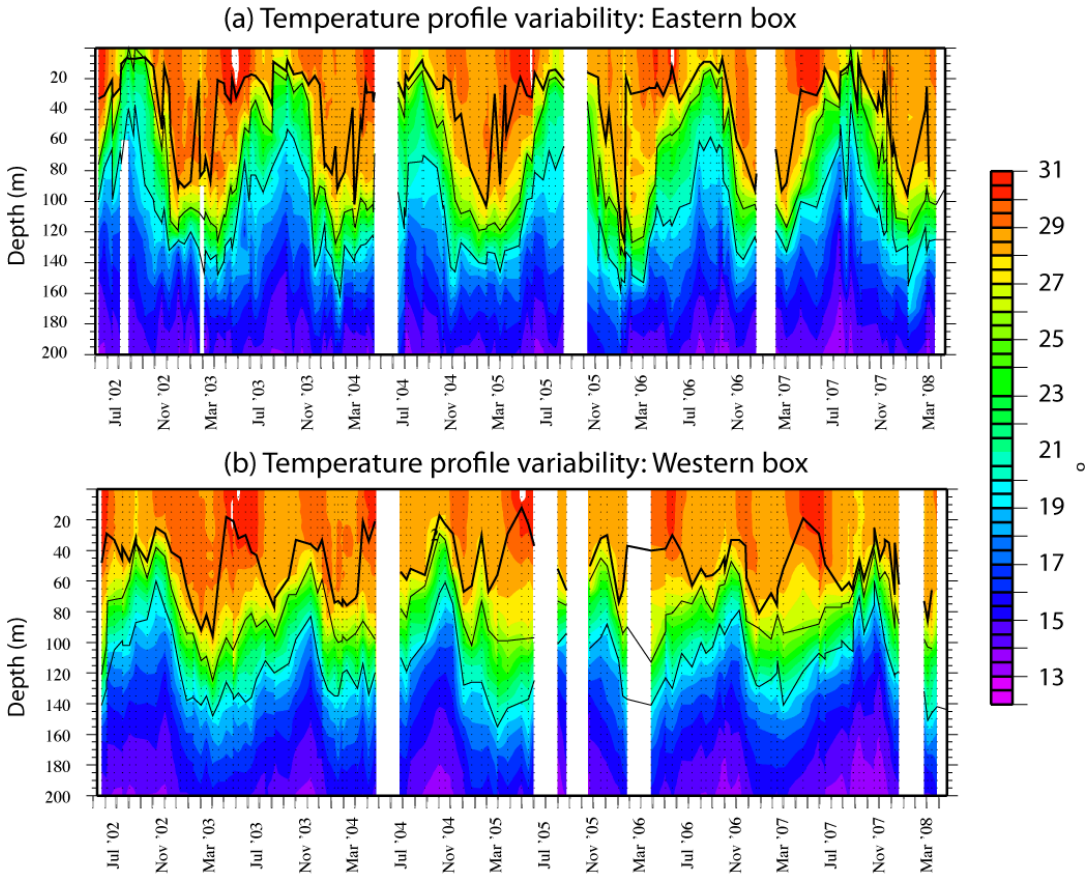
(a) Temperature profile variability: Eastern box
Depth (m)
20
40
60
80
100
120
140
160
180
200
Jul '02
Nov '02
Mar '03
Jul '03
Nov '03
Mar '04
Jul '04
Nov '04
Mar '05
Jul '05
Nov '05
Mar '06
Jul '06
Nov '06
Mar '07
Jul '07
Nov '07
Mar '08
(b) Temperature profile variability: Western box
Depth (m)
31
29
27
25
23
21
19
17
15
13
°

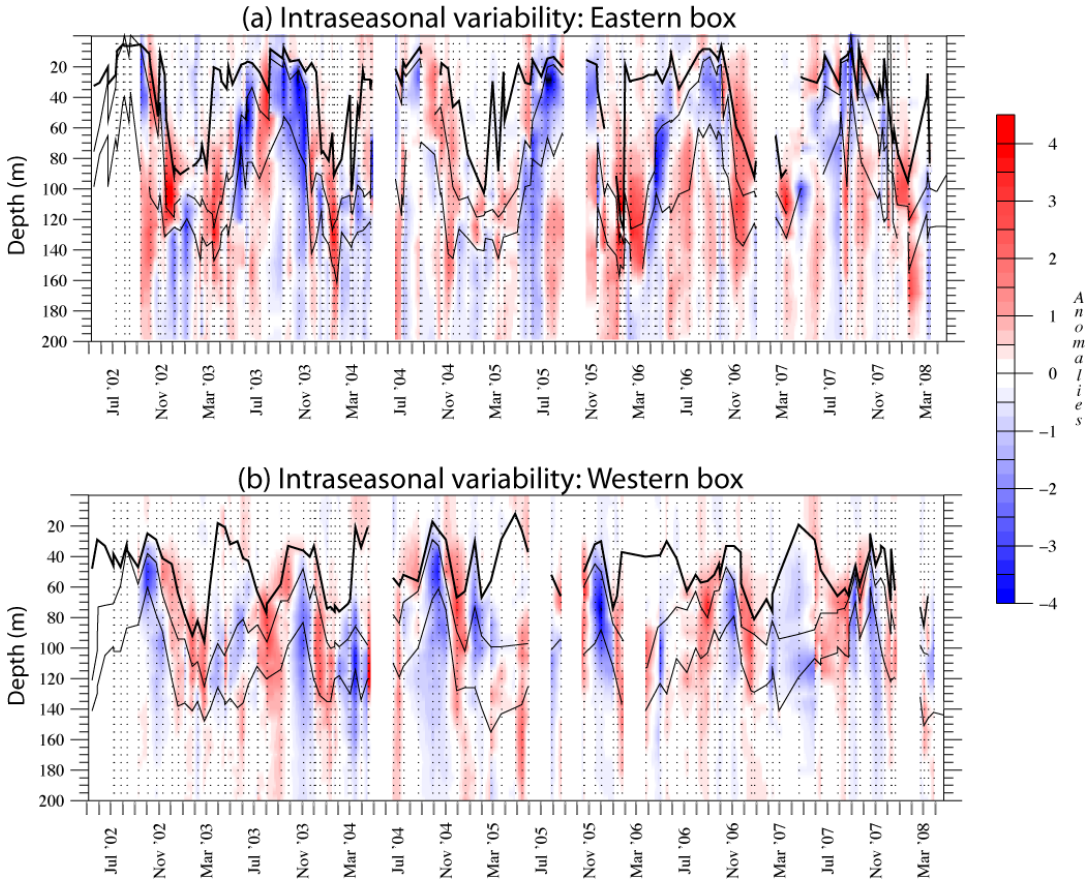
(a) Intraseasonal variability: Eastern box
(b) Intraseasonal variability: Western box
Depth (m)
20
40
60
80
100
120
140
160
180
200
Jul '02
Nov '02
Mar '03
Jul '03
Nov '03
Mar '04
Jul '04
Nov '04
Mar '05
Jul '05
Nov '05
Mar '06
Jul '06
Nov '06
Mar '07
Jul '07
Nov '07
Mar '08
4
3
2
1
0
−1
−2
−3
−4
Anomalies

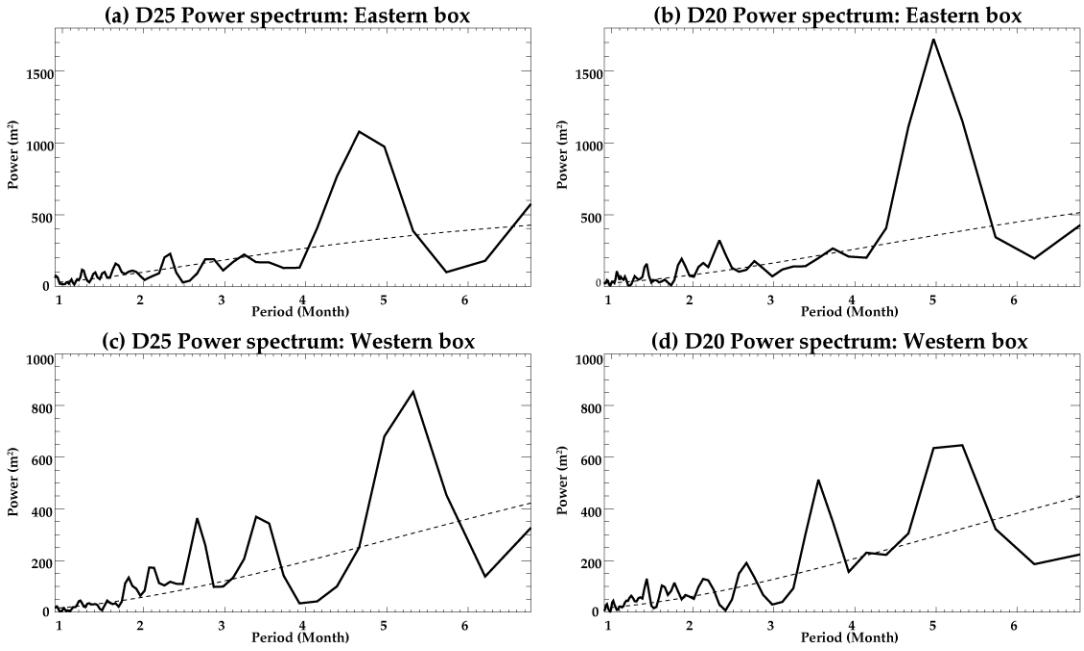
(a) D25 Power spectrum: Eastern box
(b) D20 Power spectrum: Eastern box
(c) D25 Power spectrum: Western box
(d) D20 Power spectrum: Western box
Power (m²)
Period (Month)

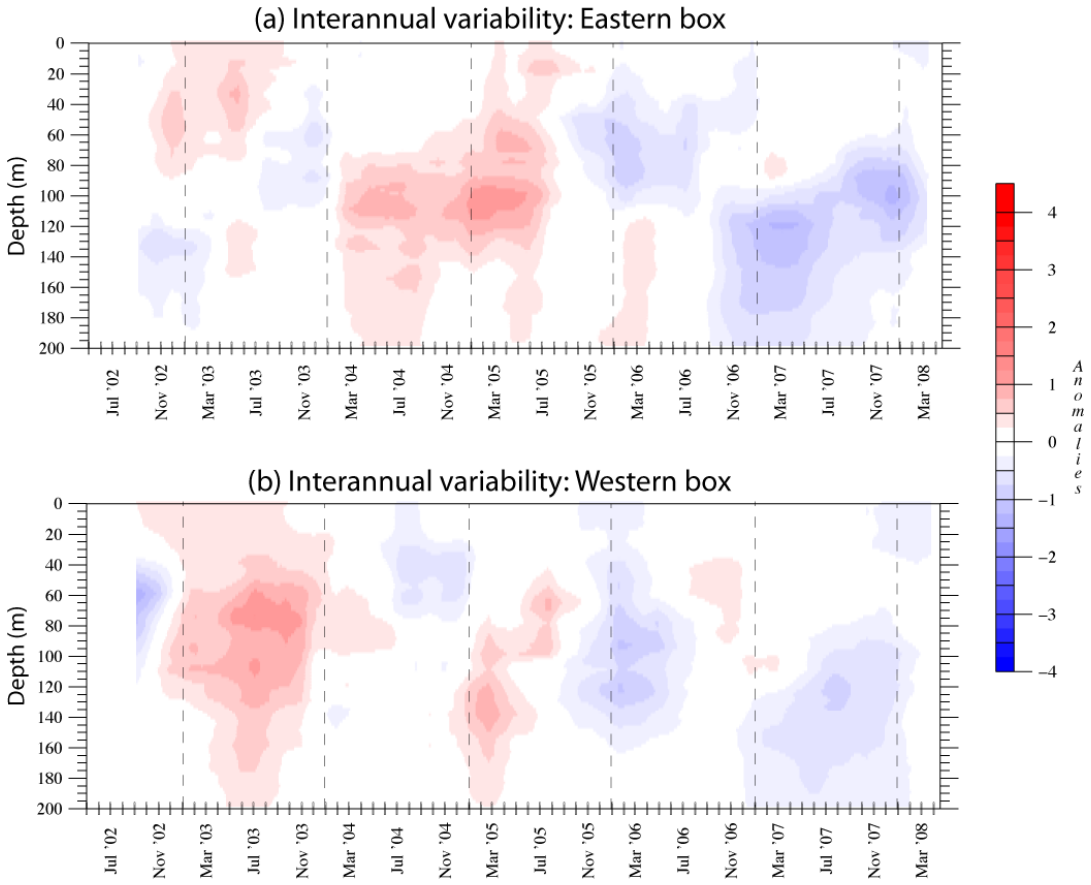
(a) Interannual variability: Eastern box
(b) Interannual variability: Western box
Depth (m)
0
20
40
60
80
100
120
140
160
180
200
Jul '02
Nov '02
Mar '03
Jul '03
Nov '03
Mar '04
Jul '04
Nov '04
Mar '05
Jul '05
Nov '05
Mar '06
Jul '06
Nov '06
Mar '07
Jul '07
Nov '07
Mar '08
4
3
2
1
0
−1
−2
−3
−4
Anomalies

Evolution of the D25 from May 2002 to April 2008

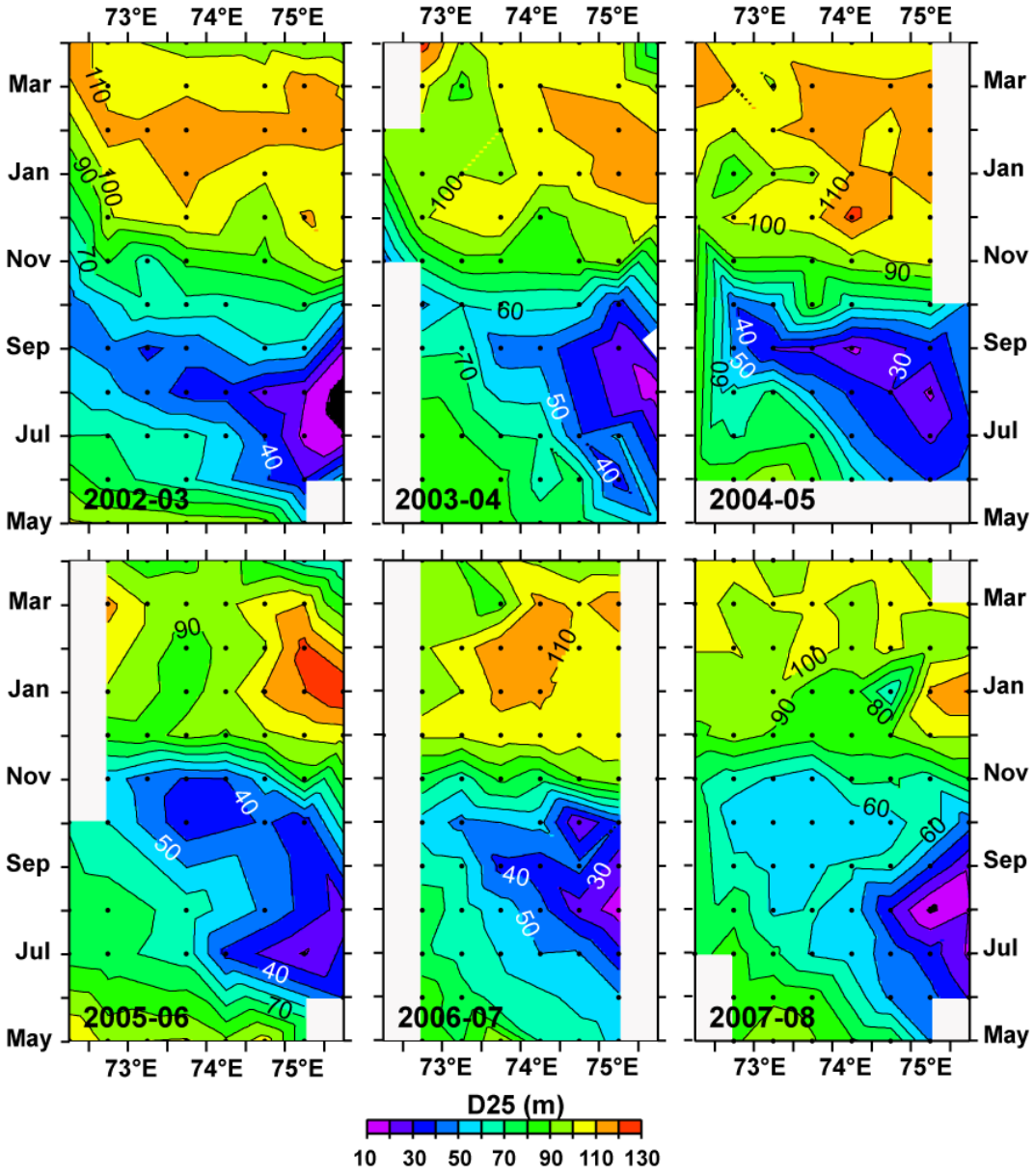

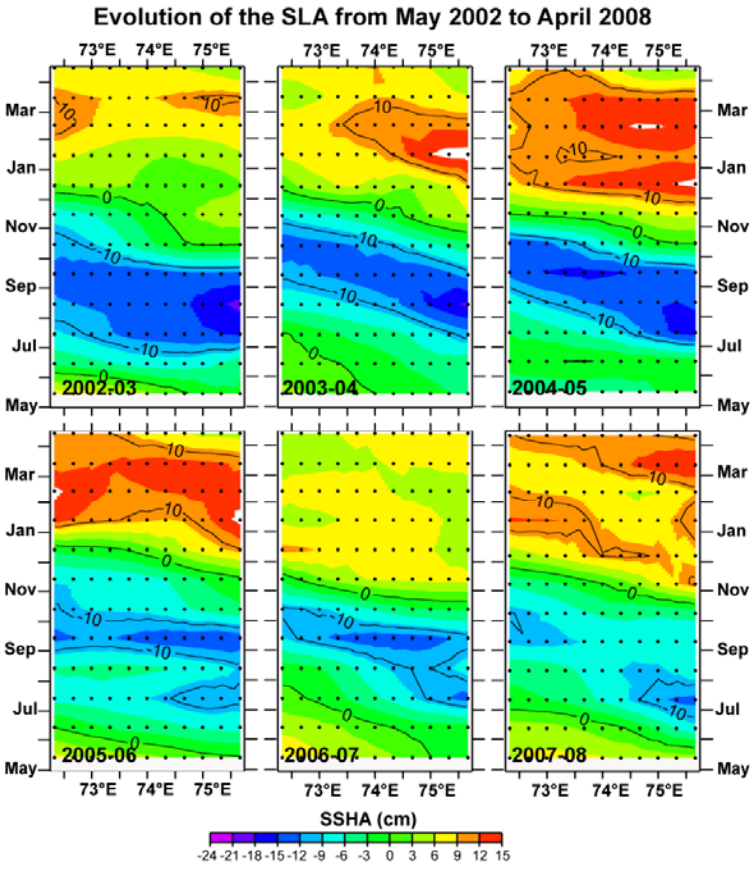
Evolution of the SLA from May 2002 to April 2008
73°E 74°E 75°E
Mar
Jan
Nov
Sep
Jul
May
2002-03
2003-04
2004-05
2005-06
2006-07
2007-08
SSHA (cm)
-24 -21 -18 -15 -12 -9 -6 -3 0 3 6 9 12 15

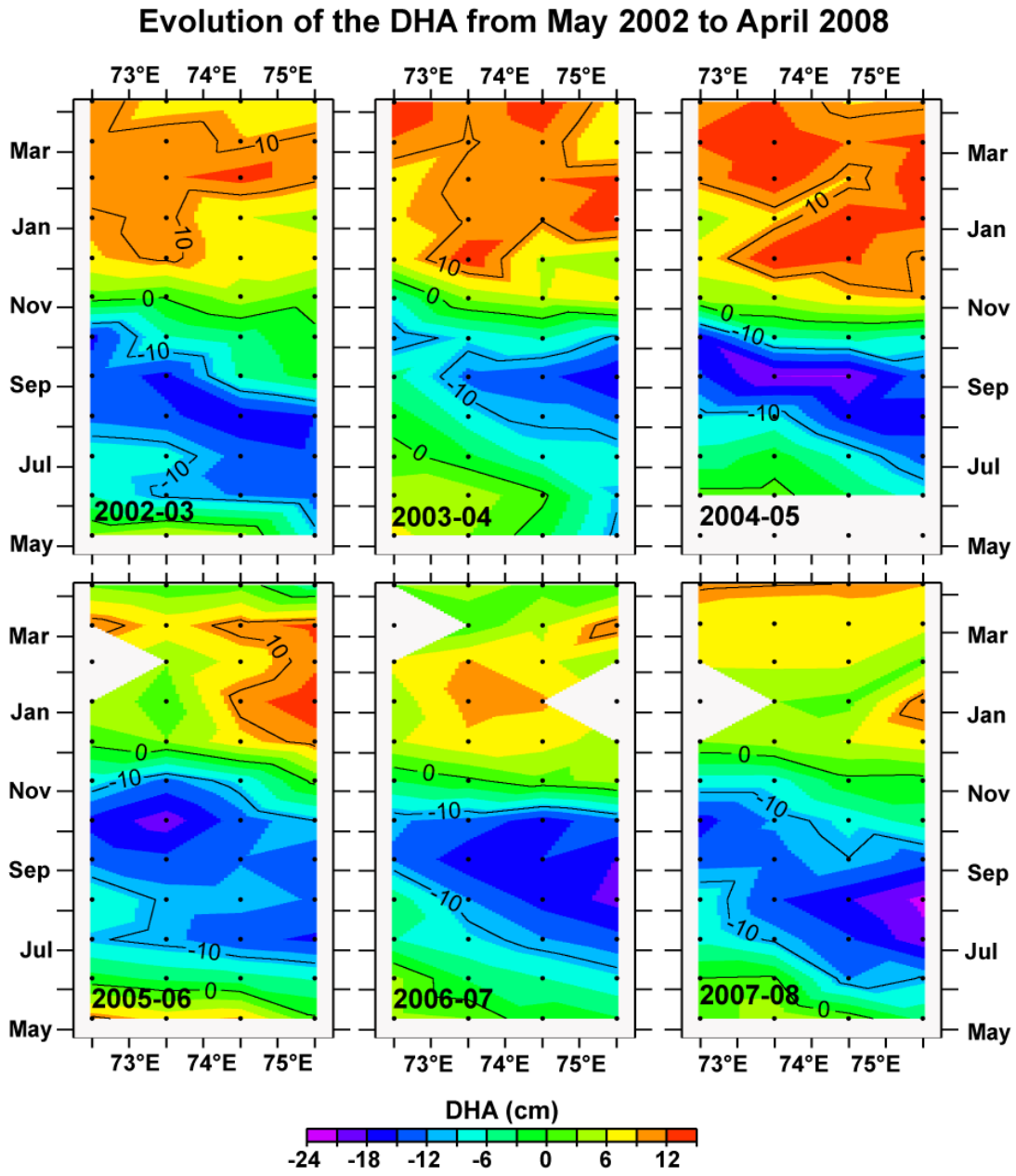
Evolution of the DHA from May 2002 to April 2008
73°E
74°E
75°E
Mar
Jan
Nov
Sep
Jul
May
2002-03
2003-04
2004-05
2005-06
2006-07
2007-08
DHA (cm)
-24
-18
-12
-6
0
6
12